Exploiting SERS Hot Spots for Disease-Specific Enzyme Detection†

ARTICLE *in* THE JOURNAL OF PHYSICAL CHEMISTRY C · DECEMBER 2009

Impact Factor: 4.77 · DOI: 10.1021/jp905493u

Exploiting SERS Hot Spots for Disease-Specific Enzyme Detection†

R. C. Maher,§ S. A. Maier, and L. F. Cohen

The Blackett Laboratory, Imperial College London Prince Consort Road, London, United Kingdom SW7 2BW

L. Koh, A. Laromaine, J. A. G. Dick, and M. M. Stevens‡

Department of Materials and Institute for Biomedical Engineering, Imperial College London, Prince Consort Road, London, United Kingdom SW7 2AZ

Received: June 11, 2009; Revised Manuscript Received: November 23, 2009

We demonstrate a method that by design reproducibly exploits hot spots in metal nanoparticle aggregates for disease-specific enzyme detection using SERS. Crucially, the reporter molecule is placed within a self-assembled bioactive gold nanostructure, at the optimal EM hot spot position, overcoming the main problem of conventional SERS-active modalities. The scheme exploits the extreme sensitivity of SERS and demonstrates the principle for a method with the potential to be highly competitive with existing immunoassay methods.

I. Introduction

The use of gold nanoparticles for the detection of biological processes using the highly chemically sensitive technique of surface-enhanced Raman scattering (SERS) has been well established since the seminal papers of Moskovits,[1,2] Emory and Nie,[3,4] and Kneipp et al.[5] Nanoparticle-based SERS has been employed for the detection and study of many biologically relevant molecules such as DNA,[6,7] proteins,[8] hemoglobin,[9] enzyme activity,[10,11] and glucose[12] as well as numerous pharmaceuticals.[13] Nevertheless, SERS hot spots have not been well exploited for commercial use. Immunoassay technology is the standard method for protein-based disease detection,[14] and any new method must have the potential to be superior not only in terms of cost or complexity of steps but also in terms of sensitivity and speed. For enzyme detection, the current medical standard delivered by the immunoassay method is on the order of 10 ng/mL.[15,16] Here, we demonstrate a method based on a colloid−molecule hybrid system engineered using bottom-up nanotechnology that has been used previously for UV−vis spectroscopy and apply it to the SERS detection method. We show that it has the potential to detect 0.003 ng/mL (10^{-13} M) and to report this information more rapidly and with fewer intervening chemical steps than the established immunoassay technology, meaning it has the potential to deliver faster, cheaper, and more reliable information for disease detection.

The SERS signal enhancement originates from intense, localized electromagnetic fields which are formed at the surfaces of metallic nanostructures when localized surface plasmons interact with incident light and scale as the fourth power of the incident field (E).[2] SERS enhancements on the order of 10^6 are typical close to the surface of a single isolated nanoparticle, but significantly larger SERS enhancements,[3,5] $\sim 10^{12}$, are present localized between two adjacent particles, which are referred to as hot spots.[2,17–21] This phenomenon is known as the coupled plasmon resonance; it is not only the dominant source of hot spot creation but also provides a route to tuning the resonance frequency.[22,23] The strong variation in enhancement means that SERS is highly sensitive to local conditions such as interparticle separation.[24,25]

Here, we demonstrate a method to control and exploit the coupled plasmon associated with a self-assembled bioactive gold nanostructure for enzyme detection. Such self-assembled structures have attracted significant interest in their own right in recent years,[26,27] and systems based on gold nanoparticles are of particular interest given that highly stable self-assembled monolayers of biologically important molecules are easily fabricated on gold surfaces by exploiting the chemical bonding between thiolated ligands and gold atoms.[28,29] Here, we use an enzyme-specific SERS reporter molecule as the linking ligand, which is a priori placed into the electromagnetic hot spot at the particle junction. One of the main drawbacks of traditional SERS-active modalities is not being able to place molecules of interest into the spatial location of hot spots and reproducibly exploit the large signal enhancement that such regions offer. The method that we describe here naturally overcomes this problem, as described below in more detail.

II. Experimental Section

Functionalization of Gold Nanoparticles with Peptides. Gold nanoparticles were functionalized following the method described in ref 30. Briefly, 40 ± 3 nm gold nanoparticles were purchased from BBI International (Agar Scientific, U.K.). The gold nanoparticles (concentrations used as received) were stabilized with 0.1 mg/mL dipotassium bis(*p*-sulfonatophenyl)phenylphosphine dihydrate for 12 h. The stabilized gold nanoparticles were stable at room temperature over a period of months. NaCl was used to precipitate the gold nanoparticles. The solution of gold nanoparticles was then centrifuged, the supernatant pulled off, and the gold nanoparticles resuspended in 10 mM potassium phosphate (pH 8) three times to remove the surfactants. Solutions of the peptide sequence terminated with a *N*-(fluorenyl-9-methoxycarbonyl) (FMOC) group (peptide: FMOC-Gly-Phe-Cys) were prepared in *N*,*N*-dimethylformamide. Peptide (20 μL of 50 μM) was added to each milliliter of a 40 nm gold nanoparticle solution with 50 μL of 2 M NaCl and left at room temperature for 19 h. Excess peptides were removed by centrifuging the functionalized gold nanoparticles

† Part of the "Martin Moskovits Festschrift".

§ E-mail: robert.maher@imperial.ac.uk.

‡ E-mail: m.stevens@imperial.ac.uk.

10.1021/jp905493u
Published on Web 12/18/2009

and removing the supernatant and replaced in 10 mM potassium phosphate (pH 8) three times.

Density Functional Theory (DFT) Calculations. The Raman spectra of the individual component amino acids of the functionalizing peptide chain were calculated using density functional theory, ignoring the influence of the gold with Gaussian 03. Calculations were carried out to the B1LYP/6311++G(d,p) level, and the calculated spectra were modified using a 0.977 scaling factor. The peptide was split into discrete sections comprised of the three amino acids (Cys, Gly, and Phe) and the FMOC to allow the calculation to be completed within a reasonable time scale.

Raman Spectroscopy. Raman spectra were collected using a Renishaw RM-2000 CCD spectrometer equipped with a Linkam temperature control stage which allowed the temperature of the sample to be controlled. Measurements in solution were made using a ×100 immersion lens index-matched to water, which was directly immersed into the sample resulting in a collection volume of approximately 5 μm^3. Measurements on dried samples were made using a high numerical aperture ×50 objective, which resulted in a laser spot of approximately 1 μm. Measurements were taken using a 633 nm HeNe laser, which delivered approximately 5mW of laser power at the focal point. For SERS monitoring of thermolysin hydrolysis on 40 nm peptide-functionalized gold nanoparticles, thermolysin solutions were freshly prepared in 10 mM potassium phosphate (pH 8) in the required concentrations. Thermolysin solutions were mixed with 300 μL of a 40 nm peptide-functionalized gold nanoparticle solution prior to acquisition of Raman spectra. Samples were monitored by the continuous collection of spectra over a 6 or more hour period. Over that time, a single spectrum was collected every 60 s after the addition of enzyme with the sample held at 37 °C to ensure optimal conditions for enzyme action. Spectral features were background-corrected and fitted to mixed Gaussian and Lorentzian modes using the Renishaw Wire software. The extracted data was further analyzed using Origin 7.5 using the integrated intensity of the 1090 cm^{-1} Raman mode of the peptide.

UV−vis Spectroscopy. Peptide-functionalized gold conjugates were prepared as described above. Excess peptide was removed by centrifugation and removal of supernatant. Gold nanoparticles were resuspended to initial volume with phosphate buffer (pH8), 0.05% w/v bovine serum albumin (BSA), and 100 mM NaCl. All spectra were collected using a Perkin−Elmer Lamda 25, over the range of 200−800 nm with 1 nm resolution at 37 °C. Background correction was performed using 10 mM phosphate buffer, 100 mM NaCl, and 0.05% w/v BSA in 1 cm path length polystyrene cuvettes. All reactions were carried out in disposable plastic cuvettes, and analysis was done in situ. Thermolysin solutions were freshly prepared in 10 mM phosphate buffer (pH 8) at the required range of units. UV-vis spectra were recorded following addition of thermolysin. The extinction spectra can be used to infer the average aggregation state of the gold nanoparticles using the ratio of the integrated signal from the dispersed and aggregated gold nanoparticles. To achieve this, the spectra were split into dispersed (D) and aggregated (A) regions, which were between 490 and 540 nm and 550 and 700 nm, respectively. The signals in these regions were then integrated, and the resulting values were used to calculate the ratio A/D. This ratio has been shown previously to be extremely sensitive to the average aggregation state of the sample and can be used to monitor the sample as a function of time.[30]

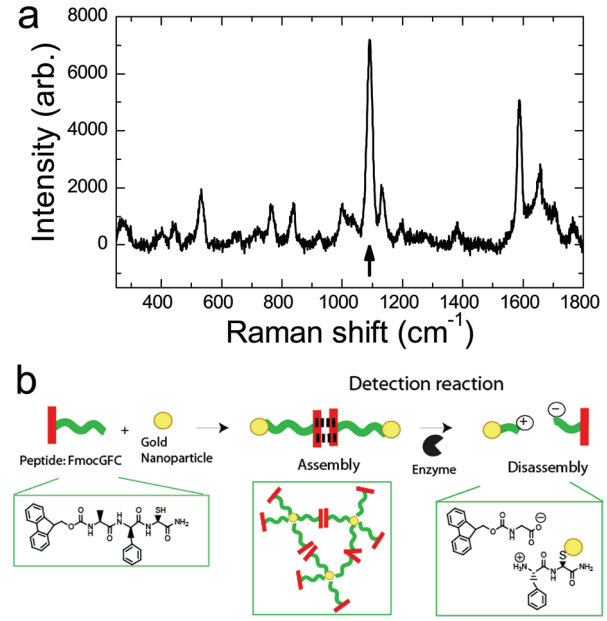

Figure 1. SERS spectrum. (a) Background-corrected Raman spectrum of the functionalized gold nanoparticles in solution obtained using 633 nm laser excitation with a 10 s integration time. The 1090 cm^{-1} peak identified by the arrow is used to monitor the enzyme activity because the peak intensity is directly related to the aggregation state of the particles. (b) Scheme for the self-assembly of the peptide-functionalized 40 nm gold nanoparticle and the deaggregation process (not to scale). Aggregation is driven by $\pi-\pi$ interactions between the FMOC groups. The gold nanoparticles are 40 nm in diameter, and the molecular chain is ∼1 nm. Dissociation of aggregates occurs upon addition of the enzyme to the solution due to the cleavage of the peptide sequence. High electromagnetic field intensities will be generated within the aggregates by the coupled plasmon interacting with the incident light. Deaggregation of the cluster occurs upon addition of the protease aided by cleavage of the peptide sequence and electrostatic repulsion. The detected SERS signal will decrease with time due to a combination of the reduction of the total number of hot spots present within the sample as well as a decrease in the intensity of those remaining hot spots as a result of increased nanoparticle separation.

III. Results and Discussion

Figure 1a shows a typical SERS spectrum obtained from a solution of gold nanoparticles functionalized with thiolated peptide sequences terminated with a FMOC group. An isolated and intense Raman mode is required for the purposes of monitoring the aggregation state of the gold nanoparticles, and the 1090 cm^{-1} Raman mode presents the ideal marker, as shown in Figure 1a.

Figure 2 shows the change in the Raman spectra observed from the functionalized gold nanoparticles before (black line) and 4 h after the addition of the 7.2 nM enzyme solution (dashed red line). There is a clear decrease in the intensity of the Raman features due to the deaggregation of the clusters caused by the action of the enzyme. The detailed process by which thermolysin cleaves these specific peptides has not been determined here, although the principle is well established.[31] In this case, the large relative size of the thermolysin (316 amino acids)[32] compared to the small peptide (3 amino acids) with which we have functionalized the gold nanoparticles might be expected to restrict enzyme activity. However, proteases are able to cleave at interfaces in vivo, and it is possible that in this case, the thermolysin cleaves peptides toward the outside of the cluster first.

It is important to understand the origins of the Raman features observed from our samples in order to optimize the sensitivity

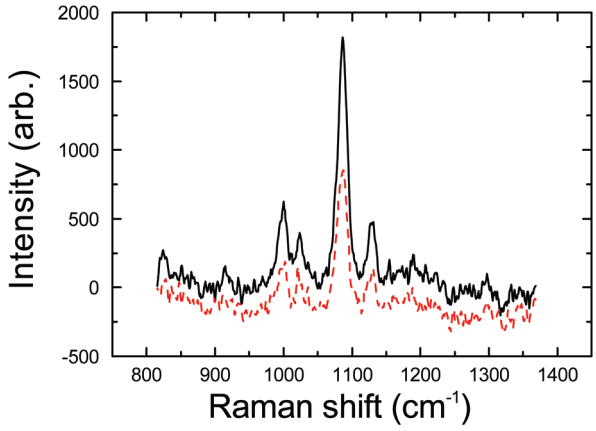

Figure 2. Raman spectra taken before (black line) and 4 h after (dashed red line) the addition of the 7.2 nM enzyme solution using the 633 nm laser with a 2 s integration time.

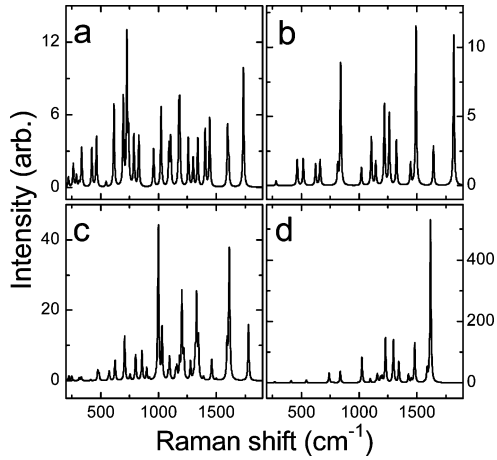

Figure 3. Raman spectra for the individual components of the functionalizing chemistry; (a) Cys, (b) Gly, (c) Phe, and (d) FMOC calculated using DFT.

TABLE 1: Integrated Raman Intensity Calculated over the Fingerprint Region (0−2000 cm^{-1}) for the Individual Component Spectra Calculated Using DFT

component	integrated intensity
Cys	1900
Gly	1023
Phe	4661
FMOC	21129

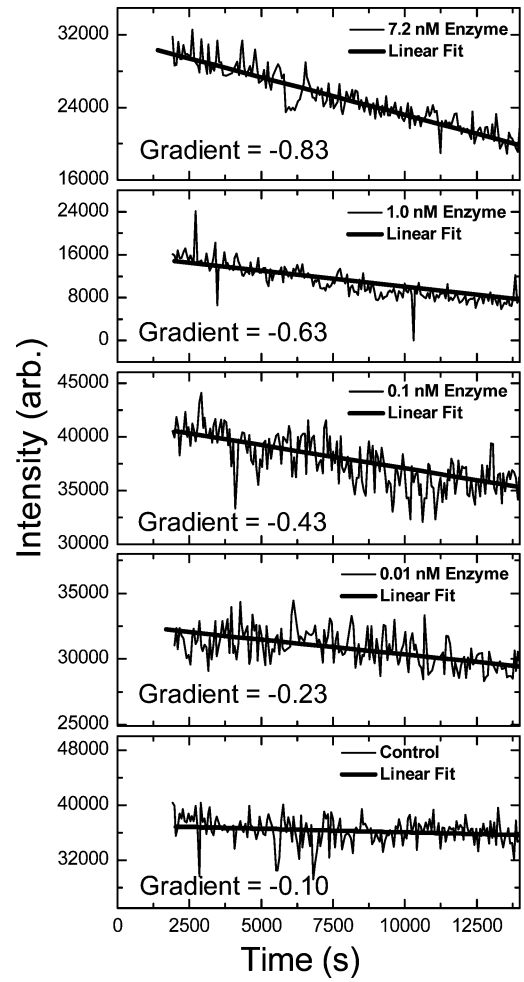

Figure 4. Monitoring the SERS intensity as a function of time. The concentration of the enzyme in solution can be deduced by measuring the change in the SERS spectrum as a function of time. The integrated intensity of the 1090 cm^{-1} FMOC Raman peak is monitored after the addition of the enzyme at concentrations of 0, 0.01, 0.1, 1.0, and 7.2 nM while the solution is held at a temperature of 37 °C. As the enzyme cleaves the functionalizing peptide, the physical binding that holds the gold nanoparticles in close proximity is destroyed, and the gold nanoparticles are isolated and positively charged, which further aids the dissociation. The integrated intensity of the 1090 cm^{-1} peak changes linearly with time, and the gradient (rate of change) is directly proportional to the enzyme concentration.

of our method. DFT calculations allow us to estimate the likely contributions from the functionalizing peptide sequence, and the calculated spectra are shown in Figure 3. These spectra are only an approximation of the Raman response from the isolated components and do not take into account the presence of the solvent, the gold, or other components of the experiment. This is illustrated by the large difference between the experimental Raman spectrum shown in Figure 1 and that calculated using DFT. However, they still serve a useful purpose in that they help to identify the likely origin of the various vibrational peaks. For example, the 1090 cm^{-1} Raman mode used in this study originates from a combination of the asymmetric stretch of the $C_\alpha-C-N$ bond, where the C_α is the C atom attached to the NH_2 group in an amide bond and the deformation of the CH aromatic ring present in the FMOC group.[33] Table 1 shows the integrated intensity over the fingerprint region of the Raman spectra from the individual components. We assign the peak to the CH aromatic ring deformation in the FMOC groups[34] because this has a significantly higher Raman cross section (by a factor of ∼10) than the $C_\alpha-C-N$ bond, as indicated by our DFT calculations.

Thus, the terminating FMOC group is the key element of the self-assembly process and acts as a reporter molecule for the SERS process. It is naturally trapped at the center of the hot spot region formed between the gold nanoparticles, as shown schematically in Figure 1b. The peptide is cleaved between the Gly and Phe amino acids by the enzyme, causing the disintegration of the nanoaggregates as a function of time (see the schematic in Figure 1b). The SERS signal of the FMOC reporter molecule drops as the self-assembled structures disassociate, with the rate of signal decrease being directly proportional to the concentration of the enzyme, as we show. The dissociation of the nanoaggregates is enhanced due to the colloids being positively charged following cleavage of the peptide. An example of the change in the Raman response is shown in Figure 2, with the initial signal from a solution prior to addition of the enzyme shown by the black curve and the red curve showing

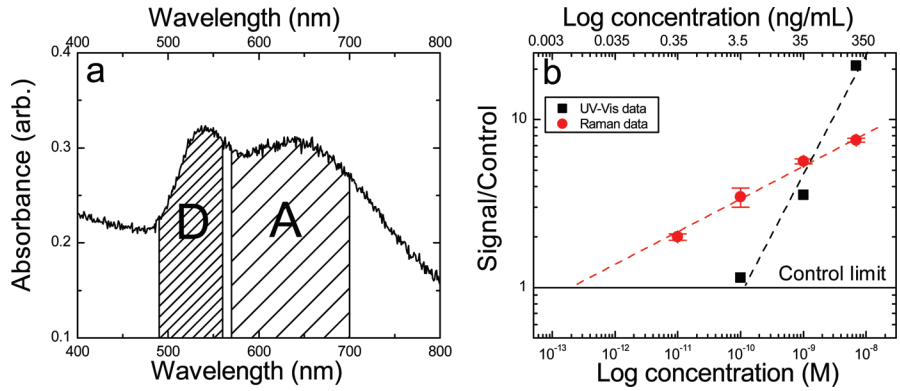

Figure 5. Comparing the detection of enzyme by UV−vis extinction and SERS. (a) The UV−vis extinction spectrum of a colloidal solution of gold nanoparticles is strongly affected by the aggregation state of the colloids. The gold nanoparticle's state affects the change (suppression) of the extinction spectrum differently in different parts of the curve. It has been shown empirically that the ratio of the integrated intensity in region D to that in region A gives an indication of nanoparticle aggregation. This method has been shown previously to allow the presence of an enzyme to be detected. In order to compare the performance of our SERS-based detection method, the action of the enzyme was monitored as a function of time using UV−vis extinction spectroscopy for the same sample parameters. (b) Both the Raman and UV−vis extinction data were then normalized to their respective control values and plotted on a logarithmic scale. The error bars associated with the measurements are within the symbol sizes, except for those of the Raman measurement at 10^{-10} M. The solid line indicates the detection limit of the two methods. The dashed lines indicate the suggested extrapolation from the measurement data points to the detection limit.

the signal 4 h after addition of the enzyme. Hence, by monitoring the intensity of the 1090 cm^{-1} peak as a function of time, it is possible to detect the presence of the enzyme. This is the basis of the detection of disease-specific enzymes using SERS hot spots, as we show in the following, where we monitor the dynamics of the interaction as a function of enzyme concentration.

Figure 4 shows the integrated intensity of the 1090 cm^{-1} peak as a function of time for various concentrations of enzyme. The gradient of this linear relationship provides the information needed to assess the sensitivity of the method once the behavior of the control sample has been taken into account. The control sample was prepared in exactly the same way, except no enzyme was added. It can be seen that the gold nanoparticles are not completely stable and a small amount of precipitation occurs with time. Fitting the control data over the measurement range shows that the signal slowly decreases with a gradient of −0.12 ± 0.02 counts/s. This represents the detection limit in this experiment. Data are shown in Figure 4 for enzyme concentrations of 0.346, 3.46, 34.6, and 249 ng/mL (which represent molar concentrations of 0.01, 0.1, 1.0, and 7.2nM). These results clearly demonstrate that the rate at which the SERS signal decreases with time is proportional to the concentration of the enzyme. The measurements have been repeated, and the results have been found to be robust.

We now compare, in terms of sensitivity and dynamic response, our SERS reporter technique as a measure of particle aggregation to more conventional and widely employed UV−vis extinction spectroscopy (or optical density measurements). The latter relies on the well-known fact that the geometry and aggregation state of the gold nanoparticles not only determine the SERS response but also other optical properties such as the extinction spectra of colloidal solutions.[35] The extinction peak red shifts upon increasing aggregation due to the coupling between individual particles, allowing the assembly and disassembly of gold nanoparticle aggregates to be monitored through a colorimetric method.[30,36–39] The basis of the technique uses two UV−vis spectral ranges shown in Figure 5a, which we label as A and D (see Experimental Section), and monitors how the ratio of the integrated intensity over these ranges varies as a function of time. To make a comparative study with the SERS results, we study the variation in the A/D ratio as a function of time for different enzyme concentrations. The variation with time was found to be linear (not shown). Table 2 summarizes the results for both the Raman and UV−vis experiments.

TABLE 2: Results of Fitting the Experimental Data Obtained from the Raman and UV−Vis Monitoring of Enzyme Induced Nanoaggregate Dispersion[a]

enzyme concentration (nM)	Raman			UV−vis A/D ratio
	$B(1)$	$B(2)$	$\langle B \rangle$	B
7.2	−0.83	−0.92	−0.87 ± 0.04	0.147
1	−0.60	−0.63	−0.62 ± 0.02	0.025
0.1	−0.43	−0.33	−0.38 ± 0.05	0.008
0.01	−0.23	−0.21	−0.22 ± 0.01	
0 (control)	−0.10	−0.14	−0.12 ± 0.02	0.007

[a] $B(1)$ and $B(2)$ represent the results of two independent measurements using the SERS method with $\langle B \rangle$ being the average.

In order to make direct comparison between the two techniques, each set is normalized to the control sample, as shown in Figure 5. At higher concentrations, the UV−vis method demonstrates a higher sensitivity, whereas at lower concentrations, the SERS method is the more sensitive. This arises due to the strong dependence of the scattering cross-section changes on the particle size. At higher enzyme concentrations, the average particle size changes more rapidly compared to lower enzyme concentrations, resulting in a large change in the UV−vis extinction. In contrast, the detected SERS signal is critically dependent on the number of hot spots, which is significant for all enzyme concentrations, and as a result, the SERS method is more sensitive for lower concentrations. A potential detection limit of 0.003 ng/mL (10^{-13} M) is suggested by the extrapolation of the results obtained, as indicated by the dashed red line in Figure 5. It must be pointed out that the UV−vis detection method has not been optimized for the use of the same 40 nm gold nanoparticles and that extremely high sensitivity has been reported previously by us for UV−vis with smaller gold particles.[30] However, in this case, we wanted a comparison with another detection method using the same system. As a result of this comparative study, we can say with confidence that the experiments that we have performed demonstrate that SERS can be used to detect the presence of the enzyme at concentrations at least 1 order of magnitude less than what is currently required for medical diagnostic applica-

tions[15] (i.e., 10^{-10} M). Moreover we can determine an unknown concentration with an accuracy governed by the reproducibility of the rate change of SERS signal intensity, which, in the application-relevant range, introduces an uncertainty in absolute value of less than 10%. Consequently, the results from the SERS technique show an extremely promising improvement in the absolute detection limit over current detection methods and demonstrate the potential of SERS for the sensitive detection of enzymes and other biologically relevant molecules.[15]

IV. Conclusions

To summarize, we have demonstrated a route to enable the detection of disease-specific enzymes at low concentrations relevant for medical diagnostic applications using self-assembled nanoaggregates of peptide−gold nanoparticle conjugates and SERS, more rapidly and with less chemical steps than current technology. The added benefit is that the design of the functionalizing chemistry is flexible and can be modified for the sensitive detection of many other disease-specific enzymes. As such, the work represents a significant step forward for the application of SERS for medical diagnostics and highlights how bottom-up nanotechnology can be employed for the implementation of hybrid nanostructures with desired functionalities.

Acknowledgment. This work has been supported by EPSRC (U.K.) under Grants EP/D063329/1 and EP/E007627/1. A.L. acknowledges Generalitat de Catalunya and EU (Beatriu de Pinos) for financial support. M.M.S. thanks the Commission of the European Communities for funding through the ERC Grant "Naturale".

References and Notes

(1) Moskovits, M. *Rev. Mod. Phys.* **1985**, *57*, 783.
(2) Moskovits, M. *J. Raman Spectrosc.* **2005**, *36*, 485.
(3) Nie, S. M.; Emory, S. R. *Science* **1997**, *275*, 1102.
(4) Emory, S. R.; Nie, S. *J. Phys. Chem. B* **1998**, *102*, 493.
(5) Kneipp, K.; Wang, Y.; Kneipp, H.; Perelman, L. T.; Itzkan, I.; Dasari, R.; Feld, M. S. *Phys. Rev. Lett.* **1997**, *78*, 1667.
(6) Cao, Y. W. C.; Jin, R. C.; Mirkin, C. A. *Science* **2002**, *297*, 1536.
(7) Vo-Dinh, T. *IEEE J. Sel. Top. Quantum Electron.* **2008**, *14*, 198.
(8) Porter, M. D.; Lipert, R. J.; Siperko, L. M.; Wang, G.; Narayanana, R. *Chem. Soc. Rev.* **2008**, *37*, 1001.
(9) Etchegoin, P.; Liem, H.; Maher, R. C.; Cohen, L. F.; Brown, R. J. C.; Milton, M. J. T.; Gallop, J. C. *Chem. Phys. Lett.* **2003**, *367*, 223.
(10) Scodeller, P.; Flexer, V.; Szamocki, R.; Calvo, E. J.; Tognalli, N.; Troiani, H.; Fainstein, A. *J. Am. Chem. Soc.* **2008**, *130*, 12690.
(11) Li, T.; Liu, D.; Wang, Z. *Biosens. Bioelectron.* **2009**, *24*, 3335.
(12) Wu, Z. S.; Zhou, G. Z.; Jiang, J. H.; Shen, G. L.; Yu, R. Q. *Talanta* **2006**, *70*, 533.
(13) Pinzaru, S. C.; Pavel, I.; Leopold, N.; Kiefer, W. *J. Raman Spectrosc.* **2004**, *35*, 338.
(14) Voller, A.; Bidwell, D. E.; Bartlett, A. *Bull. WHO* **1976**, *53*, 55.
(15) Mazhar, D.; Ngan, S.; Waxman, J. *BJU Int.* **2006**, *98*, 725.
(16) Ghadiali, J. E.; Stevens, M. M. *Adv. Mater.* **2008**, *20*, 4359.
(17) Futamata, M. *Faraday Disc.* **2006**, *132*, 45.
(18) Etchegoin, P. G.; Le Ru, E. C.; Meyer, M. *J. Chem. Phys.* **2006**, *125*, 164705.
(19) Svedberg, F.; Li, Z. P.; Xu, H. X.; Käll, M. *Nano Lett.* **2006**, *6*, 2639.
(20) Camden, J. P.; Dieringer, J. A.; Wang, Y.; Masiello, D. J.; Marks, L. D.; Schatz, G. C.; Van Duyne, R. P. *J. Am. Chem. Soc.* **2008**, *130*, 12616.
(21) Xu, H.; Aizpurua, J.; Kall, M.; Apell, P. *Phys. Rev. E* **2000**, *62*, 4318.
(22) Prodan, E.; Radloff, C.; Halas, N. J.; Nordlander, P. *Science* **2003**, *302*, 419.
(23) Maier, S. A. *Opt. Exp.* **2006**, *15*, 1957.
(24) Le Ru, E. C.; Etchegoin, P. G.; Meyer, M. *J. Chem. Phys.* **2006**, *125*, 204701.
(25) Lassiter, J. B.; Aizpurua, J.; Hernandez, L. I.; Brandl, D. W.; Romero, I.; Lal, S.; Hafner, J. H.; Nordlander, P.; Halas, N. J. *Nano Lett.* **2008**, *8*, 1212.
(26) Panyam, J.; Labhasetwar, V. *Adv. Drug Delivery Rev.* **2003**, *55*, 329.
(27) Katz, E.; Willner, I. *Ange. Chem., Int. Ed.* **2004**, *43*, 6042.
(28) Daniel, M. C.; Astruc, D. *Chem. Rev.* **2004**, *104*, 293.
(29) Freeman, R. G.; Grabar, K. C.; Allison, K. J.; Bright, R. M.; Davis, J. A.; Guthrie, A. P.; Hommer, M. B.; Jackson, M. A.; Smith, P. C.; Walter, D. G.; et al. *Science* **1995**, *267*, 1629.
(30) Laromaine, A.; Koh, L. L.; Murugesan, M.; Ulijn, R. V.; Stevens, M. M. *J. Am. Chem. Soc.* **2007**, *129*, 4156.
(31) Hangauer, D. G.; Monzingo, A. F.; Matthews, B. W. *Biochemistry* **1984**, *23*, 5730.
(32) Titani, K.; Hermodson, M. A.; Ericsson, L.; Walsh, K.; Neurath, H. *Nat. New Biol.* **1972**, *238*, 35.
(33) Podstawka, E.; Ozaki, Y.; Proniewicz, L. M. *Appl. Spectrosc.* **2005**, *59*, 1516.
(34) Socrates, G. *Infrared and Raman Characteristic Group Frequencies, Tables and Charts*; John Wiley & Sons: Chicester, U.K., 2001.
(35) Tullman, J. A.; Finney, W. F.; Lin, Y. J.; Bishnoi, S. W. *Plasmonics* **2007**, *2*, 119.
(36) Mirkin, C. A.; Letsinger, R. L.; Mucic, R. C.; Storhoff, J. J. *Nature* **1996**, *382*, 607.
(37) Faulds, K.; Littleford, R. E.; Graham, D.; Dent, G.; Smith, W. E. *Anal. Chem.* **2004**, *76*, 592.
(38) Stevens, M.; Flynn, N. T.; Wang, C.; Tirrell, D. A.; Langer, R. *Adv. Mater.* **2004**, *16*, 915.
(39) Shi, L. J.; Berkland, C. *Adv. Mater.* **2006**, *18*, 2315.

JP905493U